molecules

MDPI

Article

The Distance between Minima of Electron Density and Electrostatic Potential as a Measure of Halogen Bond Strength

Edem R. Chakalov [1], Elena Yu. Tupikina [1], Daniil M. Ivanov [1,*], Ekaterina V. Bartashevich [2] and Peter M. Tolstoy [1,*]

[1] Institute of Chemistry, St. Petersburg State University, 198504 St. Petersburg, Russia; st086266@student.spbu.ru (E.R.C.); e.tupikina@spbu.ru (E.Y.T.)
[2] Chemistry Department, South Ural State University, 454080 Chelyabinsk, Russia; bartashevichev@susu.ru
* Correspondence: d.m.ivanov@spbu.ru (D.M.I.); peter.tolstoy@spbu.ru (P.M.T.)

Abstract: In this study, we present results of a detailed topological analysis of electron density (ED) of 145 halogen-bonded complexes formed by various fluorine-, chlorine-, bromine-, and iodine-containing compounds with trimethylphosphine oxide, Me_3PO. To characterize the halogen bond (XB) strength, we used the complexation enthalpy, the interatomic distance between oxygen and halogen, as well as the typical set of electron density properties at the bond critical points calculated at B3LYP/jorge-ATZP level of theory. We show for the first time that it is possible to predict the XB strength based on the distance between the minima of ED and molecular electrostatic potential (ESP) along the XB path. The gap between ED and ESP minima exponentially depends on local electronic kinetic energy density at the bond critical point and tends to be a common limiting value for the strongest halogen bond.

Keywords: halogen bond; QTAIM; electron density; electrostatic potential; interaction energy; bond strength; density functional theory; phosphine oxide; ^{31}P NMR

Citation: Chakalov, E.R.; Tupikina, E.Yu.; Ivanov, D.M.; Bartashevich, E.V.; Tolstoy, P.M. The Distance between Minima of Electron Density and Electrostatic Potential as a Measure of Halogen Bond Strength. *Molecules* **2022**, *27*, 4848. https://doi.org/10.3390/molecules27154848

Academic Editors: Carlo Gatti and Athanassios C. Tsipis

Received: 23 June 2022
Accepted: 25 July 2022
Published: 28 July 2022

1. Introduction

Among various types of σ-hole interactions, halogen bonds (XBs) are among the most known and widely investigated [1–4]. XBs were shown to play a significant role in organocatalysis [5–8], crystal engineering and supramolecular chemistry [9–13], materials science [14–17], stabilization of explosives [18], drug design [19,20], etc. XBs R–X$\cdots$A (X—halogen) are formed between an electron-depleted region on the continuation of the R–X bond and an electron-rich region of another atom or molecule A (Figure 1, bottom). Main geometric criteria of a XB formation are the short X$\cdots$A distance, smaller than the sum of X and A van der Waals radii, and the proximity of the halogen bond angle to the linear [21]. As an electronic criterion, the presence of a critical point of type (3; −1) (bond critical point, BCP) for calculated [22–24] or experimentally measured electron density (ED) [25–28] along the X$\cdots$A bond path in QTAIM analysis (Quantum Theory of Atoms in Molecules [29]) is often used.

The philicity of halogen bonding participants can be determined using geometric criterion (the angle around electrophilic site is close to 180°) [21], spectral manifestations (for instance, in ultraviolet–visible (UV–vis) spectra [30–33] or using calculated parameters (electron density deformation (EDD) [34–40], electron localization function (ELF) distribution [41–44], natural bond orbital charge transfer [45,46], sums of atomic charges [47], and molecular electrostatic potential (ESP) distribution on the van der Waals surface with $\rho(r) = 0.001$ e/Bohr^3, in representative planes or along the bond path [48–55]).

In [54], it was mentioned for the first time for a series of hydrogen-bonded complexes that the relative arrangement of ED and ESP minima positions along the hydrogen bond path is the same for all complexes. Moreover, the superposition of gradient fields of ED and ESP as discussed for different intermolecular interactions is solids, including the

studies based on experimental charge density [56,57]. These observations formed the basis of electronic criterion proposed in Ref. [24], which makes it possible to unambiguously determine the type of electrostatically driven noncovalent bonds. In accordance with electronic criterion, the minimum of ESP along the bond path is located closer to the atom that donates electrons, whereas the minimum of ED is located closer to the atom that delivers its electrophilic site for noncovalent bonding (Figure 1). The latter atom prescribes the name of "-ogen bonds" (e.g., hydrogen, halogen, chalcogen, pnictogen, etc.).

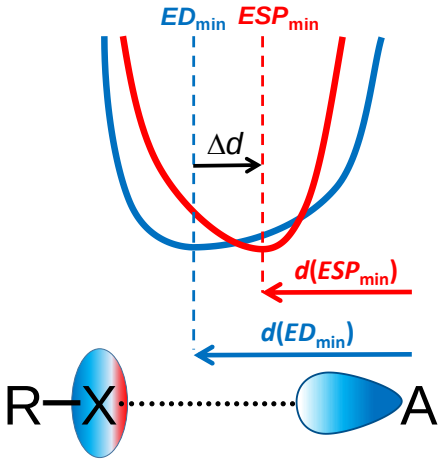

Figure 1. Schematic representation of a halogen bond (X—halogen atom, A—nucleophilic site), ED (blue) and ESP (red) distributions along the bond path. The graphical definition of $d(ED_{\min})$ (blue), $d(ESP_{\min})$ (red), and Δd (black) are given.

While for R–X···A XBs it is often clear which atom acts as an electrophile and which one acts as a nucleophile, the information value of the relative positions of ED and ESP minima seems to hold for less trivial cases of halogen-halogen contacts [58–60] and also beyond the halogen bonding in general [61,62].

Up to now, it is not known if there is an information value in the distance between ED and ESP minima, Δd, defined as

$$\Delta d = d(ED_{\min}) - d(ESP_{\min}) \quad (1)$$

(see also the graphical definition in Figure 1). A question arises: does a robust correlation exist between Δd and such XB properties as its strength or the X···A distance? To the best of our knowledge, it is an original question, not yet discussed in the QTAIM-related literature. t Of fundamental interest, we expect that this sort of information could be useful for studying XBs in solids, where ED and ESP distributions could in principle be measured experimentally [63], whereas the direct experimental evaluation of XB energy is very difficult or even not possible.

In this study, we checked the information value of Δd for a series of 145 halogen-bonded complexes formed by various halogen donors with trimethylphosphine oxide, Me_3PO (Figure 2) at the B3LYP/jorge-ATZP level of theory. The Me_3PO molecule was chosen as a "standard" halogen acceptor, in a sense following the approach started many years ago by Gutmann and Beckett [64,65] and explored in recent years by a number of authors [66–68]. In order to reduce the number of internal degrees of freedom in the electron donor, we have selected Me_3PO instead of Et_3PO, which was originally used in the Gutmann–Beckett method. As halogen donors the molecules belonging to the following classes of F-, Cl-, Br- and I-containing compounds were considered: halogens, interhalides, oxohalides, pseudohalides, halogenated methane, ethylene, acetylene, benzene, phosgene and their derivatives, as well as thionyl- and sulfurylhalides, sulfur halides and sulfur hypohalites, and several halogenated nitrogen-containing inorganic compounds and some others. This choice of model systems makes it possible to track how a change in the halogen bond acceptor (i.e., its electronic prop-

erties as well as belonging to a certain class of chemical compounds) changes the properties of the halogen bond when the halogen bond acceptor Me_3PO is fixed. The full list of halogen donors is given in Figure S1 in Supplementary Materials.

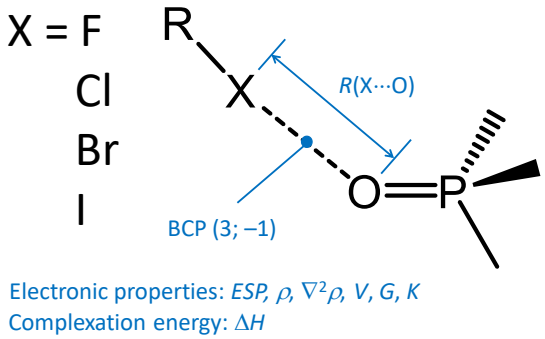

Figure 2. Schematic representation of halogen-bonded complexes formed between R–X (X = F, Cl, Br and I) and Me_3PO. In blue are given geometric (interatomic distance $R(X\cdots O)$), energetic (complexation enthalpy ΔH), and electronic (ρ stands for electron density, $\nabla^2\rho$ for its Laplacian, V, G and K stand for local electron potential, kinetic and total energy densities at the bond critical point, BCP) parameters that were correlated with Δd in this work (see Figure 1 for the definition of Δd).

Previously, we have considered a similar but somewhat smaller set of complexes in order to build a correlation between the XB strength/geometry and the changes of two spectral parameters upon complexation: the ^{31}P NMR chemical shift and the ν(P=O) stretching frequency [69] (similar correlations for hydrogen-bonded complexes with Me_3PO were recently published as well [70]). We have shown that decent correlations of this kind do exist, and they could be fitted by simple analytical functions. Now, we turn our attention to electronic properties, such as Δd, which is experimentally accessible—if the conditions are right—for single crystal samples. Several XB parameters were considered in this work and correlated with Δd: the complexation enthalpy ΔH, the X$\cdots$O interatomic distance $R(X\cdots O)$, and various parameters at XB electron density critical point of type (3; −1): (molecular electrostatic potential $ESP(r_{BCP})$, electron density $\rho(r_{BCP})$, Laplacian of electron density $\nabla^2\rho(r_{BCP})$, local electron kinetic $G(r_{BCP})$ and potential $V(r_{BCP})$ energy densities and total electron energy density $K(r_{BCP})$). We also checked if ^{31}P NMR chemical shifts of Me_3PO correlate with Δd.

2. Results and Discussion

The optimized geometries of some representative examples of halogen-bonded complexes belonging to different classes of inorganic and organic compounds are shown in Figure 3 and all 145 halogen-bonded complexes are shown in Supplementary Materials (Figure S1). The majority of XBs are linear (or close to linear) and formed along the direction of expected oxygen lone pair localization. The numerical values of relevant parameters are listed in Supplementary Materials: geometric, energetic and spectroscopic parameters (Table S1), and QTAIM electronic parameters (Table S2).

Figure 4a shows the dependence of distances from oxygen to ESP and ED minima—$d(ESP_{min})$ and $d(ED_{min})$, respectively—along the XB path as a function of the local electron kinetic energy density at critical point of type (3; −1), $G(r_{BCP})$ (in kJ/(mol·Å^3)), taken as a measure of XB strength. In Figure S2 (Supplementary Materials) we show several examples of ED and ESP profiles along the bond path for weak, medium, and strong R–Cl$\cdots$OPMe$_3$ complexes. The $d(ESP_{min})$ distance is among the largest ones for free Me_3PO (see the black dot in Figure 4a) and falls upon the increase in the XB strength. The $d(ED_{min})$ is obviously infinite for free Me_3PO, but rapidly—quasi-exponentially—decreases when the XB gets stronger. The $d(ESP_{min})$ and $d(ED_{min})$ values appear to be almost halogen-independent, except for complexes with F-donors, the $d(ESP_{min})$ data points for which deviate consistently from the other sets.

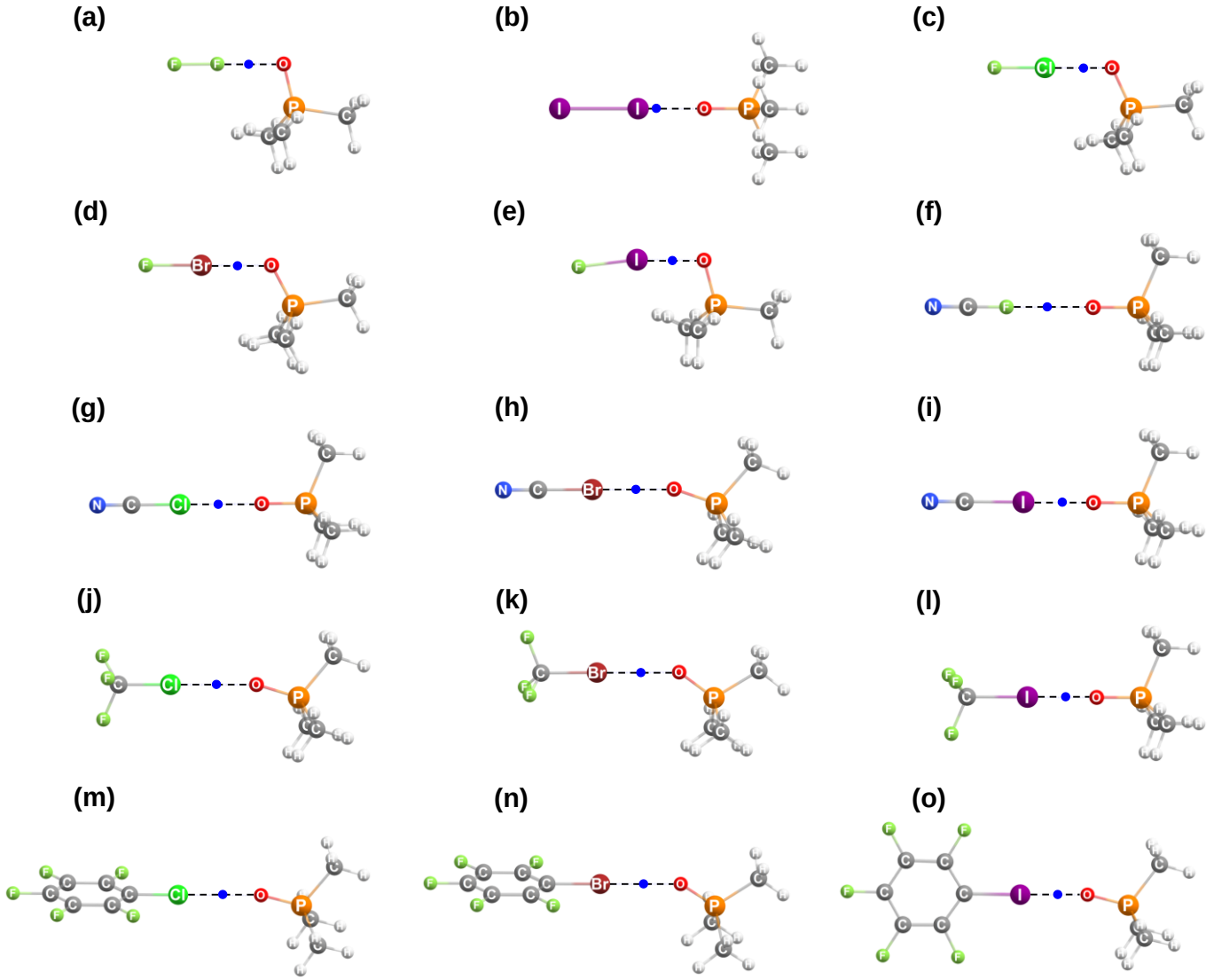

Figure 3. Some examples of optimized geometries of halogen-bonded complexes formed between (**a**) F_2; (**b**) I_2; (**c**) ClF; (**d**) BrF; (**e**) IF; (**f**) FCN; (**g**) ClCN; (**h**) BrCN; (**i**) ICN; (**j**) CF_3Cl; (**k**) CF_3Br; (**l**) CF_3I; (**m**) C_6F_5Cl; (**n**) C_6F_5Br; (**o**) C_6F_5I and Me_3PO considered in this work. Blue dot marks the position of the X···O bond critical point.

However, a closer look at the $\Delta d = d(ESP_{min}) - d(ED_{min})$ values (Figure 4b) reveals that there are some systematic differences between complexes with Cl-, Br-, and I-donors as well. The general trend is the same for all halogens: the stronger is the XB, the closer are the ESP and ED minima. The Δd values within each series seem to approach a limiting (asymptotic) value for the strongest XBs. A question arises, what are the limiting Δd values for hypothetical strongest possible bonds? As models for such X···O bonds, we took cations Me_3POX^+, the optimized geometries of which together with the X···O bond parameters are shown in Figure S3. For these cations, the "asymptotic" $G(r_{BCP})$ values are the largest and Δd values are the smallest within the respective series of complexes (except for complexes with iodine, where there is a significant scattering of data points for strong XBs). We have added Δd asymptotes as horizontal bold lines in Figure 4b. For F-donors, the Δd even gets slightly negative, suggesting that the electrophile/nucleophile roles are practically swapped for the F–O bond in Me_3POF^+, as compared to non-covalent R–X···$OPMe_3$ complexes (i.e., the F–O bond in Me_3POF^+ cannot be classified as a halogen bond).

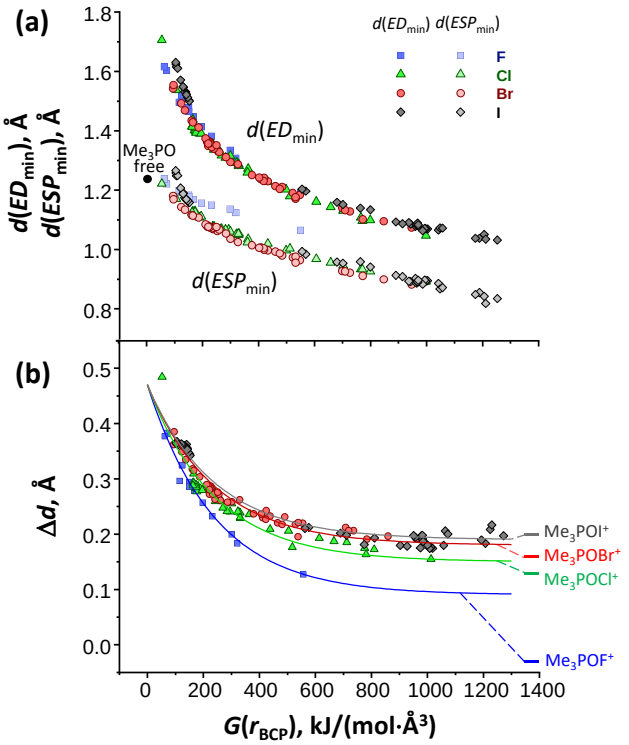

Figure 4. (**a**) Distances from oxygen atom to minima of molecular electrostatic potential $d(ESP_{min})$ (lighter colors) and electron density $d(ED_{min})$ (darker colors) along the X···O (X = F, Cl, Br and I) bond path; (**b**) distances between ED and ESP minima Δd as a function of $G(r_{BCP})$ for a series of halogen-bonded complexes formed between R–X and Me_3PO. The solid curves correspond to Equation (2) with fitted parameters listed in Table 1.

Table 1. Fitting parameters a_X, Δd_0 and b for Equation (2) and proportionality coefficient k between $G(r_{BCP})$ and complexation energy ΔE (Equation (4) [69]) for the data sets plotted in Figure 4b.

Halogen Donor	a_X, Å	Δd_0, Å	b, kJ/(mol·Å^3)	k, Å^3
F	0.09	0.47	240	0.18
Cl	0.15	0.47	240	0.47
Br	0.18	0.47	240	0.57
I	0.19	0.47	240	0.74

The data sets in the Δd plot versus $G(r_{BCP})$ for the studied sets of halogen-bonded complexes could be reasonably well fitted, assuming an overall exponential behavior:

$$\Delta d = a_X + (\Delta d_0 - a_X) \cdot \exp(-G(r_{BCP})/b). \quad (2)$$

Interestingly, only one fitting parameter in Equation (2), a_X, is halogen-dependent (see Table 1). The rate of exponential fall b = 240 kJ/(mol·Å^3) and the limiting Δd value for $G(r_{BCP})$ = 0 kJ/(mol·Å^3), Δd_0 = 0.47 Å, seem to be virtually the same for all halogens. At the moment, it is not clear if these values for Δd_0 and b reflect some property of Me_3PO or a property of XBs in general. The result of the fitting is added to Figure 4b as solid lines. Another noteworthy thing is that the fitting with Equation (2) does not reproduce the asymptotic values for Me_3POX^+ at $G(r_{BCP}) \to \infty$, though the relative position of the fitting asymptotes for F, Cl, Br and I is the same as for the corresponding cations Me_3POX^+. Solving Equation (2) for $G(r_{BCP})$ one obtains

$$G(r_{BCP}) = b \cdot \ln\left(\frac{\Delta d_0 - a_X}{\Delta d - a_X}\right). \quad (3)$$

It should be noted that Equation (3) makes sense only when the logarithm is defined ($\Delta d > a_X$) and positive ($\Delta d < \Delta d_0$). This means that Equation (3) might become inapplicable for extremely weak and extremely strong XBs. Subsequently, the $G(r_{BCP})$ values could be converted into the XB "complexation energies" ΔE (the difference of total electronic energies of the complex and its isolated relaxed constituents) using previously published halogen-dependent proportionality coefficients k (see the last column in Table 1; the values were taken from Table 2 in Ref. [69]),

$$\Delta E = k \cdot G(r_{BCP}). \quad (4)$$

At this point, it is worth making a brief comment concerning various quantitative models based on the properties of electron density at the bond critical points, which were previously successfully used for characterization of the energy for various types of noncovalent bonds [70–75]. Figure S4 shows the correlation between the complexation enthalpy ΔH and $G(r_{BCP})$. Note that there is a significant scattering of the data points due to the fact that a number of complexes within the studied series are held not only by an XB, but also by other noncovalent interactions, most prominently weak hydrogen bonds between electronegative atoms of the halogen donor (including the halogen itself) and the methyl protons of the Me_3PO moiety (Figure 5). For completeness of the subject, in Figures S5–S8 we show also correlations of electron density $\rho(r_{BCP})$, Laplacian of electron density $\nabla^2\rho(r_{BCP})$ and total electron energy density $K(r_{BCP}) = G(r_{BCP}) + V(r_{BCP})$ with $d(ESP_{min})$, $d(ED_{min})$, Δd, and R_{norm}, as well as $G(r_{BCP})$ correlation with $V(r_{BCP})$, $\rho(r_{BCP})$, $\nabla^2\rho(r_{BCP})$ and $ESP(r_{BCP})$. In turn, Figure S9 shows ΔH, $\rho(r_{BCP})$, $\nabla^2\rho(r_{BCP})$ and $ESP(r_{BCP})$ dependence on Δd.

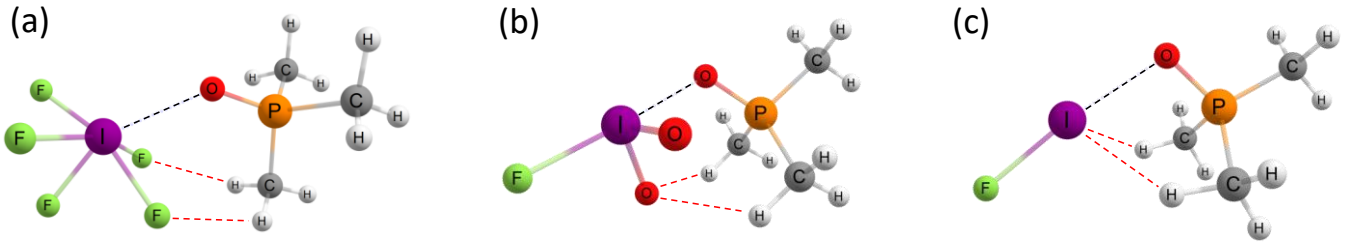

Figure 5. Examples of additional non-covalent interactions (red dashed lines) present in some halogen-bonded (black dashed line) R–X···$OPMe_3$ complexes: hydrogen bonds between methyl protons of the Me_3PO moiety and electronegative atoms of the halogen donor; (**a**) two H-bonds with two proton acceptors; (**b**) two H-bonds with one proton acceptor; (**c**) two H-bonds with the halogen donating atom.

Finally, the Δd values are plotted in Figure 6 as a function of R_{norm}, defined as X···O interatomic distance, normalized by the sum of van der Waals radii (R_{vdW}) of X (X = F, Cl, Br and I) and O:

$$R_{norm} = \frac{R(X \cdots O)}{R_{vdW}(X) + R_{vdW}(O)}, \quad (5)$$

where the following values of the van der Waals radii were used: 1.52 Å (O), 1.47 Å (F), 1.75 Å (Cl), 1.85 Å (Br), 1.98 Å (I) [76]. The usage of normalized and unitless R_{norm}, instead of direct interatomic distances X···O, allows one—at least in principle—to compare XBs with participation of different halogens (see the dependence of absolute R(X···O) distances and R_{norm} on $G(r_{BCP})$ in Figure S10). The data sets plotted in Figure 6 indicate slightly non-linear dependencies of Δd on R_{norm} for each halogen, but generally show the same trends as Figure 4b, because the terms halogen bond strength and shortness are almost interchangeable: stronger/shorter XBs are characterized by smaller Δd values.

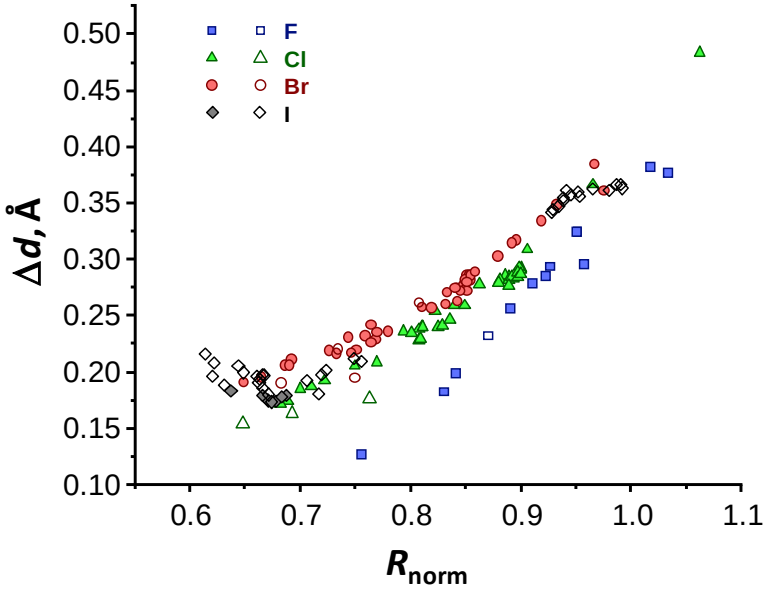

Figure 6. Distances between ED and ESP minima Δd as a function of normalized interatomic distances R_{norm} between X (X = F, Cl, Br and I) and O (see definition in Equation (5)).

To summarize the results so far, there is indeed a correlation between Δd and XB energy and length. The exponential fall of Δd upon strengthening/shortening of the XB is dependent on the type of halogen and most probably on the type of the electron-donating atom as well (oxygen in our case), but for a fixed pair of atoms the correlations seem to be largely independent on the substituents, which makes Δd a promising tool in characterization of XBs and—speculatively—other types of non-covalent interactions as well.

Now we turn attention to the spectroscopic manifestation of halogen bonding within the studied series of complexes. In Ref. [69], some of us have demonstrated that isotropic ^{31}P NMR chemical shift of Me_3PO could be used as a spectroscopic marker for the halogen-donating ability of a probed molecule or, in other words, as a measure of the XB strength (length) in a R–X$\cdots$OPMe$_3$ complex. For the data sets presented in this work, reasonable correlations between the change of the ^{31}P NMR chemical shift upon complexation $\Delta\delta^{31}$P and the complexation enthalpy ΔH exist for chlorine- and bromine-containing complexes (Figure S11a). For fluorine- and iodine-containing ones, there is a large scattering of the data points, which in case of complexes with iodine is likely to be—at least partially—due to the presence of additional non-covalent interactions and, consequently, the influence of several competing factors (e.g., presence of additional interactions) on the electron shells of the phosphorus atom. Indeed, the $\Delta\delta^{31}$P correlation with $G(r_{BCP})$ values (Figure S11b) is noticeably better, though with significant residual scattering still (it should be mentioned, that the shape of $\Delta\delta^{31}$P(Δd) remains the same upon the change of a basis set).

Figure 7 shows the correlation of $\Delta\delta^{31}$P with Δd, which has a similar degree of data point scattering as Figure S11b. Because of that, we have added to Figure 7 two trend curves for chlorine- and bromine-containing complexes only. These curves serve only as guides for the eye, as it seems premature to propose a functional fit. Still, one could confirm that ^{31}P NMR chemical shift sensitively reflect the changes in the electronic structure of the complexes—including the parameter in focus of this work, Δd—and could serve for the characterization of XBs with phosphine oxides.

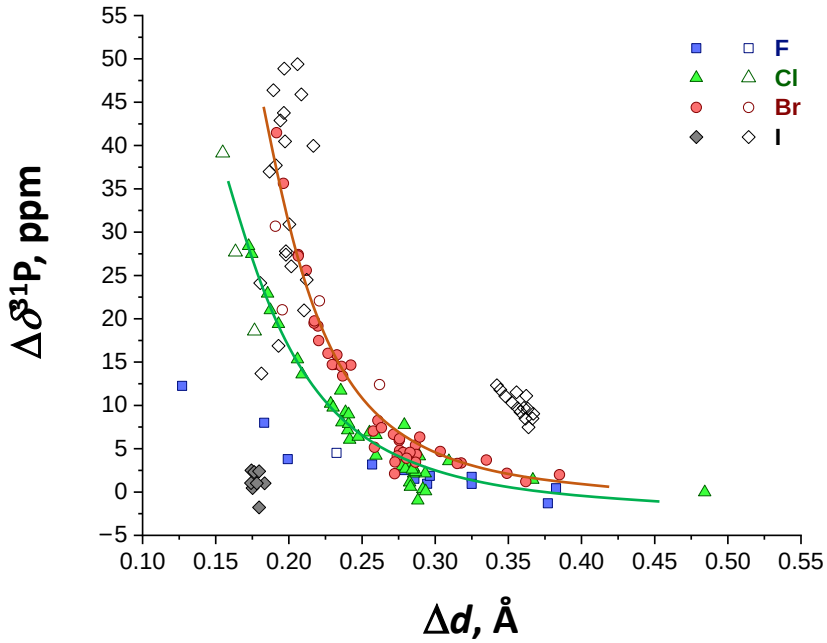

Figure 7. The correlation of $\Delta\delta^{31}$P on Δd for a series of R–X$\cdots$OPMe$_3$ complexes. The solid lines are guides for the eye added for Cl- and Br-bonded complexes.

3. Computational Methods

The full geometry optimization, harmonic vibrational frequencies and NMR calculations were performed for studied complexes in vacuum using B3LYP functional [77] and nonrelativistic all-electron augmented triple-zeta valence quality basis set with polarization functions jorge-ATZP [78–80] (adopted from the Basis Set Exchange site [81]) using Gaussian16 software package [82]. Geometry optimization was performed using the default for Gaussian16 Berny algorithm without any geometry restrictions and standard convergence criteria (maximum/RMS forces and displacements of atoms smaller than 0.000450 a.u./0.000300 a.u. and 0.001800 a.u./0.001200 a.u., respectively). The optimized geometries were checked for the absence of imaginary vibrational frequencies. The presence of halogen bonds in the calculated complexes was confirmed by the criteria for halogen bond formation, according to the IUPAC recommendation [21]. For each halogen donor, only one optimized structure of its complex with phosphine oxide was considered. For a subset of complexes, we have checked that variations in the initial geometries lead to the same optimized structures. Because of this, we believe that they are true global minima. However, even if it is not the case, any local true minimum containing a halogen bond and satisfying the Virial theorem would be legitimate structure to perform topological analysis of electron density and use the resulting data to construct correlations.

The complexation enthalpy ΔH was calculated at 298.15 K as the enthalpy required to separate the interacting molecules at infinite distance (including the relaxation of monomers). Note that in this way the ΔH values include contributions not only from the XB, but also from any other non-covalent interactions which might be present between monomers of Me_3PO and XB donor.

Isotropic NMR shielding constants σ were calculated using the gauge-independent atomic orbital (GIAO) approach [83] and converted into changes of chemical shifts upon complexation as $\Delta\delta^{31}P = \sigma_{free} - \sigma$, where σ_{free} is the ^{31}P nuclear shielding constant for an isolated Me_3PO molecule.

The topological analysis of ED and ESP along the XB path was carried out within the framework of QTAIM methodology from the wave function files using MultiWFN software (http://sobereva.com/multiwfn/ accessed on 22 June 2022; Beijing Kein Research Center for Natural Sciences; Beijing, China; version 3.3.8) [84]. The ED and ESP minima positions from the oxygen atom along the XB path were determined with the following

path searching parameters: maximum number of points of a path is 100000, with stepsize of 0.0005 Bohr and generation stop threshold of 0.005 Bohr distance to any critical point. This takes into account that for all studied complexes $d(ESP_{min}) < d(ED_{min})$, the definition given in Equation (1) makes all Δd values positive.

Visualization of the studied complexes was performed using the Chemcraft software (available online at www.chemcraftprog.com accessed on 22 June 2022; version 1.8) [85].

All of the proposed correlation functions were fitted by Levenberg–Marquardt algorithm and visualized using Origin software (OriginLab Corporation, Northampton, MA, USA) [86]. The complexes with X···H (X = N, O, F, Cl, Br or I; H are protons of methyl groups) contacts shorter than the sum of Bondi's van der Waals radii of corresponding atoms are marked in red in the Supplementary Materials (Figure S1 and Tables S1 and S2).

4. Conclusions

The summary and the main conclusion of this work are rather concise. For a homologous series of 145 halogen-bonded complexes with the general formula R–X···$OPMe_3$ (X = F, Cl, Br, and I), we showed that the XB strength/energy correlate well with the distance between ED and ESP minima along the X···O bond path, Δd (see Equation (2); Figure 4b). The maximum Δd value (for weakest XBs) as well as the exponent of the fall of the Δd dependence on $G(r_{BCP})$ are halogen-independent, whereas the limiting values for strongest XBs are halogen-dependent. One could expect that there is also a dependence on the type of electron-donating atom (here, oxygen), though this and other limits of applicability of the proposed correlations remain to be studied. Quite likely, the most robust conclusion one could make is that for a pair of homologous non-covalently bound complexes the one with larger Δd is weaker. The numerical value of Δd might appear to be useful in analysis of experimental high-resolution X-ray data on ED of halogen-bonded single crystals. We also propose Δd as a new tool for routine QTAIM analysis of the energies of XBs.

Supplementary Materials: The following supporting information can be downloaded at: https://www.mdpi.com/article/10.3390/molecules27154848/s1. Figure S1: optimized structures of R–X···$OPMe_3$ complexes; Table S1: normalized R_{norm} and absolute R(X···O) distances, valence bond angles α(R–X···O) and β(X···O–P), changes of ^{31}P NMR chemical shifts upon complexation $\Delta\delta^{31}$P, and complexation energies ΔH and ΔG; Table S2: minima positions of ED and ESP, $d(ED_{min})$ and $d(ESP_{min})$, along the XB path and distance between them Δd, and QTAIM parameters at XB critical point of type (3; −1) ($\rho(r_{BCP})$, $\nabla^2\rho(r_{BCP})$, $G(r_{BCP})$, $V(r_{BCP})$, $K(r_{BCP})$); Figure S2: ED and ESP profiles along the XB path for weak, medium, and strong R–Cl···$OPMe_3$ complexes; Figure S3: optimized structures of Me_3POX^+ (X = F, Cl, Br, and I) complexes; Figure S4: ΔH as a function of $G(r_{BCP})$; Figures S5–S7: $d(ESP_{min})$, $d(ED_{min})$, Δd, and R_{norm} as functions of electron density $\rho(r_{BCP})$, Laplacian of electron density $\nabla^2\rho(r_{BCP})$, and total electron energy density $K(r_{BCP})$ at XB critical point of type (3; –1); Figure S8: $V(r_{BCP})$, $\rho(r_{BCP})$, $\nabla^2\rho(r_{BCP})$, and $ESP(r_{BCP})$ as functions of $G(r_{BCP})$; Figure S9: ΔH, $\rho(r_{BCP})$, $\nabla^2\rho(r_{BCP})$, and $ESP(r_{BCP})$ as functions of Δd; Figure S10: R_{norm} and R(X···O) as functions of $G(r_{BCP})$; Figure S11: ΔH and $G(r_{BCP})$ as functions of $\Delta\delta^{31}$P.

Author Contributions: Investigation, E.R.C.; Visualization, E.R.C.; Validation, E.Y.T.; Supervision, E.Y.T., P.M.T. and E.V.B.; Methodology, E.V.B.; Conceptualization, D.M.I. and P.M.T.; Writing—Original Draft Preparation, D.M.I. and P.M.T.; Funding Acquisition, P.M.T. All authors have read and agreed to the published version of the manuscript.

Funding: This work was supported by the Russian Science Foundation (project 18-13-00050).

Institutional Review Board Statement: Not applicable.

Informed Consent Statement: Not applicable.

Data Availability Statement: All data are available within the article or Supplementary Materials.

Acknowledgments: Authors acknowledges the Computer Center of St. Petersburg University Research Park for providing computational resources.

Conflicts of Interest: The authors declare no conflict of interest.

Sample Availability: Samples of the compounds are available from the authors.

References

1. Politzer, P.; Lane, P.; Concha, M.C.; Ma, Y.; Murray, J.S. An Overview of Halogen Bonding. *J. Mol. Model.* **2007**, *13*, 305–311. [CrossRef] [PubMed]
2. Politzer, P.; Murray, J.S.; Clark, T. Halogen Bonding: An Electrostatically-Driven Highly Directional Noncovalent Interaction. *Phys. Chem. Chem. Phys.* **2010**, *12*, 7748–7757. [CrossRef] [PubMed]
3. Wang, C.; Danovich, D.; Mo, Y.; Shaik, S. On the Nature of the Halogen Bond. *J. Chem. Theory Comput.* **2014**, *10*, 3726–3737. [CrossRef] [PubMed]
4. Cavallo, G.; Metrangolo, P.; Milani, R.; Pilati, T.; Priimagi, A.; Resnati, G.; Terraneo, G. The Halogen Bond. *Chem. Rev.* **2016**, *116*, 2478–2601. [CrossRef] [PubMed]
5. Yang, H.; Wong, M.W. Application of Halogen Bonding to Organocatalysis: A Theoretical Perspective. *Molecules* **2020**, *25*, 1045. [CrossRef] [PubMed]
6. Sutar, R.L.; Huber, S.M. Catalysis of Organic Reactions through Halogen Bonding. *ACS Catal.* **2019**, *9*, 9622–9639. [CrossRef]
7. Wang, C.G.; Chong, A.M.L.; Pan, H.M.; Sarkar, J.; Tay, X.T.; Goto, A. Recent Development in Halogen-Bonding-Catalyzed Living Radical Polymerization. *Polym. Chem.* **2020**, *11*, 5559–5571. [CrossRef]
8. Tepper, R.; Schubert, U.S. Halogen Bonding in Solution: Anion Recognition, Templated Self-Assembly, and Organocatalysis. *Angew. Chem. Int. Ed.* **2018**, *57*, 6004–6016. [CrossRef]
9. Metrangolo, P.; Neukirch, H.; Pilati, T.; Resnati, G. Halogen Bonding Based Recognition Processes: A World Parallel to Hydrogen Bonding. *Acc. Chem. Res.* **2005**, *38*, 386–395. [CrossRef]
10. Priimagi, A.; Cavallo, G.; Metrangolo, P.; Resnati, G. The Halogen Bond in the Design of Functional Supramolecular Materials: Recent Advances. *Acc. Chem. Res.* **2013**, *46*, 2686–2695. [CrossRef]
11. Nemec, V.; Lisac, K.; Bedeković, N.; Fotović, L.; Stilinović, V.; Cinčić, D. Crystal Engineering Strategies towards Halogen-Bonded Metal-Organic Multi-Component Solids: Salts, Cocrystals and Salt Cocrystals. *CrystEngComm* **2021**, *23*, 3063–3083. [CrossRef]
12. Mukherjee, A.; Tothadi, S.; Desiraju, G.R. Halogen Bonds in Crystal Engineering: Like Hydrogen Bonds yet Different. *Acc. Chem. Res.* **2014**, *47*, 2514–2524. [CrossRef]
13. Ivanov, D.M.; Bokach, N.A.; Kukushkin, V.Y.; Frontera, A. Metal Centers as Nucleophiles: Oxymoron of Halogen Bond-Involving Crystal Engineering. *Chemistry* **2022**, *28*, e202103173. [CrossRef]
14. Saccone, M.; Catalano, L. Halogen Bonding beyond Crystals in Materials Science. *J. Phys. Chem. B* **2019**, *123*, 9281–9290. [CrossRef]
15. Berger, G.; Frangville, P.; Meyer, F. Halogen Bonding for Molecular Recognition: New Developments in Materials and Biological Sciences. *Chem. Commun.* **2020**, *56*, 4970–4981. [CrossRef]
16. Zheng, J.; Suwardi, A.; Wong, C.J.E.; Loh, X.J.; Li, Z. Halogen Bonding Regulated Functional Nanomaterials. *Nanoscale Adv.* **2021**, *3*, 6342–6357. [CrossRef]
17. Biswas, S.; Das, A. Recent Developments in Polymeric Assemblies and Functional Materials by Halogen Bonding. *ChemNanoMat* **2021**, *7*, 748–772. [CrossRef]
18. Landenberger, K.B.; Bolton, O.; Matzger, A.J. Energetic-Energetic Cocrystals of Diacetone Diperoxide (DADP): Dramatic and Divergent Sensitivity Modifications via Cocrystallization. *J. Am. Chem. Soc.* **2015**, *137*, 5074–5079. [CrossRef]
19. Baldrighi, M.; Cavallo, G.; Chierotti, M.R.; Gobetto, R.; Metrangolo, P.; Pilati, T.; Resnati, G.; Terraneo, G. Halogen Bonding and Pharmaceutical Cocrystals: The Case of a Widely Used Preservative. *Mol. Pharm.* **2013**, *10*, 1760–1772. [CrossRef] [PubMed]
20. Xu, Z.; Yang, Z.; Liu, Y.; Lu, Y.; Chen, K.; Zhu, W. Halogen Bond: Its Role beyond Drug-Target Binding Affinity for Drug Discovery and Development. *J. Chem. Inf. Model.* **2014**, *54*, 69–78. [CrossRef]
21. Desiraju, G.R.; Ho, P.S.; Kloo, L.; Legon, A.C.; Marquardt, R.; Metrangolo, P.; Politzer, P.; Resnati, G.; Rissanen, K. Definition of the Halogen Bond (IUPAC Recommendations 2013). *Pure Appl. Chem.* **2013**, *85*, 1711–1713. [CrossRef]
22. Wick, C.R.; Clark, T. On Bond-Critical Points in QTAIM and Weak Interactions. *J. Mol. Model.* **2018**, *24*, 142. [CrossRef] [PubMed]
23. Syzgantseva, O.A.; Tognetti, V.; Joubert, L. On the Physical Nature of Halogen Bonds: A QTAIM Study. *J. Phys. Chem. A* **2013**, *117*, 8969–8980. [CrossRef] [PubMed]
24. Bartashevich, E.; Mukhitdinova, S.; Yushina, I.; Tsirelson, V. Electronic Criterion for Categorizing the Chalcogen and Halogen Bonds: Sulfur–Iodine Interactions in Crystals. *Acta Crystallogr. Sect. B Struct. Sci. Cryst. Eng. Mater.* **2019**, *75*, 117–126. [CrossRef]
25. Pavan, M.S.; Durga Prasad, K.; Guru Row, T.N. Halogen Bonding in Fluorine: Experimental Charge Density Study on Intermolecular F···F and F···S Donor–Acceptor Contacts. *Chem. Commun.* **2013**, *49*, 7558. [CrossRef]
26. Chua, Z.; Zarychta, B.; Gianopoulos, C.G.; Zhurov, V.V.; Pinkerton, A.A. Revisiting the Charge Density Analysis of 2,5-Dichloro-1,4-Benzoquinone at 20 K. *Acta Crystallogr. Sect. B Struct. Sci. Cryst. Eng. Mater.* **2017**, *73*, 654–659. [CrossRef]
27. Eraković, M.; Cinčić, D.; Molčanov, K.; Stilinović, V. A Crystallographic Charge Density Study of the Partial Covalent Nature of Strong N···Br Halogen Bonds. *Angew. Chem. Int. Ed.* **2019**, *58*, 15702–15706. [CrossRef]
28. Bianchi, R.; Forni, A.; Pilati, T. Experimental Electron Density Study of the Supramolecular Aggregation between 4,4′-Dipyridyl-N, N′-Dioxide and 1,4-Diiodotetrafluorobenzene at 90 K. *Acta Crystallogr. Sect. B Struct. Sci.* **2004**, *60*, 559–568. [CrossRef]
29. Bader, R.F.W. *Atoms in Molecules. A Quantum Theory*; Clarendon Press: Oxford, UK, 1994.

30. Rosokha, S.V.; Stern, C.L.; Ritzert, J.T. Experimental and Computational Probes of the Nature of Halogen Bonding: Complexes of Bromine-Containing Molecules with Bromide Anions. *Chemistry* **2013**, *19*, 8774–8788. [CrossRef]
31. Rosokha, S.V.; Traversa, A. From Charge Transfer to Electron Transfer in Halogen-Bonded Complexes of Electrophilic Bromocarbons with Halide Anions. *Phys. Chem. Chem. Phys.* **2015**, *17*, 4989–4999. [CrossRef]
32. Rosokha, S.V.; Vinakos, M.K. Hybrid Network Formation via Halogen Bonding of the Neutral Bromo-Substituted Organic Molecules with Anionic Metal–Bromide Complexes. *Cryst. Growth Des.* **2012**, *12*, 4149–4156. [CrossRef]
33. Weinberger, C.; Hines, R.; Zeller, M.; Rosokha, S.V. Continuum of Covalent to Intermolecular Bonding in the Halogen-Bonded Complexes of 1,4-Diazabicyclo[2.2.2]Octane with Bromine-Containing Electrophiles. *Chem. Commun.* **2018**, *54*, 8060–8063. [CrossRef]
34. Coppens, P.; Stevens, E.D. Accurate X-Ray Diffraction and Quantum Chemistry: The Study of Charge Density Distributions. *Adv. Quantum Chem.* **1977**, *10*, 1–35. [CrossRef]
35. Cremer, D.; Kraka, E. Chemical Bonds without Bonding Electron Density ? Does the Difference Electron-Density Analysis Suffice for a Description of the Chemical Bond? *Angew. Chem. Int. Ed. Engl.* **1984**, *23*, 627–628. [CrossRef]
36. Schwarz, W.H.E.; Ruedenberg, K.; Mensching, L. Chemical Deformation Densities. 1. Principles and Formulation of Quantitative Determination. *J. Am. Chem. Soc.* **1989**, *111*, 6926–6933. [CrossRef]
37. Mensching, L.; Von Niessen, W.; Valtazanos, P.; Ruedenberg, K.; Schwarz, W.H.E. Chemical Deformation Densities. 2. Small Molecules. *J. Am. Chem. Soc.* **1989**, *111*, 6933–6941. [CrossRef]
38. Blanco, F.; Alkorta, I.; Rozas, I.; Solimannejad, M.; Elguero, J. A Theoretical Study of the Interactions of NF3 with Neutral Ambidentate Electron Donor and Acceptor Molecules. *Phys. Chem. Chem. Phys.* **2011**, *13*, 674–683. [CrossRef]
39. Solimannejad, M.; Malekani, M.; Alkorta, I. Cooperativity between the Hydrogen Bonding and Halogen Bonding in F3CX···NCH(CNH)···NCH(CNH) Complexes (X = Cl, Br). *Mol. Phys.* **2011**, *109*, 1641–1648. [CrossRef]
40. Bartashevich, E.V.; Tsirelson, V.G. Interplay between Non-Covalent Interactions in Complexes and Crystals with Halogen Bonds. *Russ. Chem. Rev.* **2014**, *83*, 1181–1203. [CrossRef]
41. Becke, A.D.; Edgecombe, K.E. A Simple Measure of Electron Localization in Atomic and Molecular Systems. *J. Chem. Phys.* **1990**, *92*, 5397–5403. [CrossRef]
42. Silvi, B.; Savin, A. Classification of Chemical Bonds Based on Topological Analysis of Electron Localization Functions. *Nature* **1994**, *371*, 683–686. [CrossRef]
43. Savin, A.; Nesper, R.; Wengert, S.; Fässler, T.F. ELF: The Electron Localization Function. *Angew. Chem. Int. Ed. Engl.* **1997**, *36*, 1808–1832. [CrossRef]
44. Bulatova, M.; Ivanov, D.M.; Rautiainen, J.M.; Kinzhalov, M.A.; Truong, K.N.; Lahtinen, M.; Haukka, M. Studies of Nature of Uncommon Bifurcated I–I···(I–M) Metal-Involving Noncovalent Interaction in Palladium(II) and Platinum(II) Isocyanide Cocrystals. *Inorg. Chem.* **2021**, *60*, 13200–13211. [CrossRef] [PubMed]
45. Weinhold, F.; Landis, C.R. Natural Bond Orbitals and Extensions of Localized Bonding Concepts. *Chem. Educ. Res. Pract.* **2001**, *2*, 91–104. [CrossRef]
46. Reed, A.E.; Curtiss, L.A.; Weinhold, F. Intermolecular Interactions from a Natural Bond Orbital, Donor-Acceptor Viewpoint. *Chem. Rev.* **1988**, *88*, 899–926. [CrossRef]
47. Sadlej-Sosnowska, N. Transfer of Electron Density as a Result of Hydrogen Bond Formation. *Int. J. Quantum Chem.* **2009**, *109*, 294–300. [CrossRef]
48. Scrocco, E.; Tomasi, J. Electronic Molecular Structure, Reactivity and Intermolecular Forces: An Euristic Interpretation by Means of Electrostatic Molecular Potentials. *Adv. Quantum Chem.* **1978**, *11*, 115–193. [CrossRef]
49. Brammer, L.; Bruton, E.A.; Sherwood, P. Understanding the Behavior of Halogens as Hydrogen Bond Acceptors. *Cryst. Growth Des.* **2001**, *1*, 277–290. [CrossRef]
50. Lu, T.; Chen, F. Revealing the Nature of Intermolecular Interaction and Configurational Preference of the Nonpolar Molecular Dimers $(H_2)_2$, $(N_2)_2$, and $(H_2)(N_2)$. *J. Mol. Model.* **2013**, *19*, 5387–5395. [CrossRef]
51. Kolář, M.; Hostaš, J.; Hobza, P. The Strength and Directionality of a Halogen Bond Are Co-Determined by the Magnitude and Size of the σ-Hole. *Phys. Chem. Chem. Phys.* **2014**, *16*, 9987–9996. [CrossRef]
52. Heidrich, J.; Exner, T.E.; Boeckler, F.M. Predicting the Magnitude of σ-Holes Using VmaxPred, a Fast and Efficient Tool Supporting the Application of Halogen Bonds in Drug Discovery. *J. Chem. Inf. Model.* **2019**, *59*, 636–643. [CrossRef]
53. Brinck, T.; Murray, J.S.; Politzer, P. Surface Electrostatic Potentials of Halogenated Methanes as Indicators of Directional Intermolecular Interactions. *Int. J. Quantum Chem.* **1992**, *44*, 57–64. [CrossRef]
54. Mata, I.; Molins, E.; Alkorta, I.; Espinosa, E. Topological Properties of the Electrostatic Potential in Weak and Moderate N···H Hydrogen Bonds. *J. Phys. Chem. A* **2007**, *111*, 6425–6433. [CrossRef]
55. Zelenkov, L.E.; Eliseeva, A.A.; Baykov, S.V.; Suslonov, V.V.; Galmés, B.; Frontera, A.; Kukushkin, V.Y.; Ivanov, D.M.; Bokach, N.A. Electron Belt-to-σ-Hole Switch of Noncovalently Bound Iodine(i) Atoms in Dithiocarbamate Metal Complexes. *Inorg. Chem. Front.* **2021**, *8*, 2505–2517. [CrossRef]
56. Tsirelson, V.G.; Avilov, A.S.; Lepeshov, G.G.; Kulygin, A.K.; Stahn, J.; Pietsch, U.; Spence, J.C.H. Quantitative Analysis of the Electrostatic Potential in Rock-Salt Crystals Using Accurate Electron Diffraction Data. *J. Phys. Chem. B* **2002**, *105*, 5068–5074. [CrossRef]

57. Tsirelson, V.G.; Shishkina, A.V.; Stash, A.I.; Parsons, S. The Experimental and Theoretical QTAIMC Study of the Atomic and Molecular Interactions in Dinitrogen Tetroxide. *Acta Crystallogr. Sect. B Struct. Sci.* **2009**, *65*, 647–658. [CrossRef]
58. Dabranskaya, U.; Ivanov, D.M.; Novikov, A.S.; Matveychuk, Y.V.; Bokach, N.A.; Kukushkin, V.Y. Metal-Involving Bifurcated Halogen Bonding C-Br$\cdots\eta^2$(Cl-Pt). *Cryst. Growth Des.* **2019**, *19*, 1364–1376. [CrossRef]
59. Lamberts, K.; Handels, P.; Englert, U.; Aubert, E.; Espinosa, E. Stabilization of Polyiodide Chains via Anion$\cdots$anion Interactions: Experiment and Theory. *CrystEngComm* **2016**, *18*, 3832–3841. [CrossRef]
60. Kashina, M.V.; Ivanov, D.M.; Kinzhalov, M.A. The Isocyanide Complexes Cis-[$MCl_2(CNC_6H_4$-4-X$)_2$] (M = Pd, Pt; X = Cl, Br) as Tectons in Crystal Engineering Involving Halogen Bonds. *Crystals* **2021**, *11*, 799. [CrossRef]
61. Bartashevich, E.V.; Matveychuk, Y.V.; Mukhitdinova, S.E.; Sobalev, S.A.; Khrenova, M.G.; Tsirelson, V.G. The Common Trends for the Halogen, Chalcogen, and Pnictogen Bonds via Sorting Principles and Local Bonding Properties. *Theor. Chem. Acc.* **2020**, *139*, 26. [CrossRef]
62. Bartashevich, E.; Matveychuk, Y.; Tsirelson, V. Identification of the Tetrel Bonds between Halide Anions and Carbon Atom of Methyl Groups Using Electronic Criterion. *Molecules* **2019**, *24*, 1083. [CrossRef]
63. Abramov, Y.A. On the Possibility of Kinetic Energy Density Evaluation from the Experimental Electron-Density Distribution. *Acta Crystallogr. Sect. A Found. Crystallogr.* **1997**, *53*, 264–272. [CrossRef]
64. Mayer, U.; Gutmann, V.; Gerger, W. The Acceptor Number—A Quantitative Empirical Parameter for the Electrophilic Properties of Solvents. *Mon. Chem.* **1975**, *106*, 1235–1257. [CrossRef]
65. Beckett, M.A.; Brassington, D.S.; Coles, S.J.; Hursthouse, M.B. Lewis Acidity of Tris(Pentafluorophenyl) Borane: Crystal and Molecular Structure of B(C6F5)3·OPEt3. *Inorg. Chem. Commun.* **2000**, *3*, 530–533. [CrossRef]
66. McCune, J.A.; He, P.; Petkovic, M.; Coleman, F.; Estager, J.; Holbrey, J.D.; Seddon, K.R.; Swadźba-Kwaśny, M. Brønsted Acids in Ionic Liquids: How Acidity Depends on the Liquid Structure. *Phys. Chem. Chem. Phys.* **2014**, *16*, 23233–23243. [CrossRef]
67. Osegovic, J.P.; Drago, R.S. Measurement of the Global Acidity of Solid Acids by 31P MAS NMR of Chemisorbed Triethylphosphine Oxide. *J. Phys. Chem. B* **2000**, *104*, 147–154. [CrossRef]
68. Zheng, A.; Liu, S.B.; Deng, F. 31P NMR Chemical Shifts of Phosphorus Probes as Reliable and Practical Acidity Scales for Solid and Liquid Catalysts. *Chem. Rev.* **2017**, *117*, 12475–12531. [CrossRef]
69. Ostras, A.S.; Ivanov, D.M.; Novikov, A.S.; Tolstoy, P.M. Phosphine Oxides as Spectroscopic Halogen Bond Descriptors: IR and NMR Correlations with Interatomic Distances and Complexation Energy. *Molecules* **2020**, *25*, 1406. [CrossRef]
70. Kostin, M.A.; Pylaeva, S.A.; Tolstoy, P.M. Phosphine Oxides as NMR and IR Spectroscopic Probes for the Estimation of the Geometry and Energy of PO$\cdots$H–A Hydrogen Bonds. *Phys. Chem. Chem. Phys.* **2022**, *24*, 7121–7133. [CrossRef] [PubMed]
71. Espinosa, E.; Alkorta, I.; Elguero, J.; Molins, E. From Weak to Strong Interactions: A Comprehensive Analysis of the Topological and Energetic Properties of the Electron Density Distribution Involving X-H$\cdots$F-Y Systems. *J. Chem. Phys.* **2002**, *117*, 5529–5542. [CrossRef]
72. Espinosa, E.; Molins, E.; Lecomte, C. Hydrogen Bond Strengths Revealed by Topological Analyses of Experimentally Observed Electron Densities. *Chem. Phys. Lett.* **1998**, *285*, 170–173. [CrossRef]
73. Spackman, M.A. How Reliable Are Intermolecular Interaction Energies Estimated from Topological Analysis of Experimental Electron Densities? *Cryst. Growth Des.* **2015**, *15*, 5624–5628. [CrossRef]
74. Alkorta, I.; Legon, A.C. Nucleophilicities of Lewis Bases b and Electrophilicities of Lewis Acids a Determined from the Dissociation Energies of Complexes B$\cdots$A Involving Hydrogen Bonds, Tetrel Bonds, Pnictogen Bonds, Chalcogen Bonds and Halogen Bonds. *Molecules* **2017**, *22*, 1786. [CrossRef] [PubMed]
75. Bikbaeva, Z.M.; Ivanov, D.M.; Novikov, A.S.; Ananyev, I.V.; Bokach, N.A.; Kukushkin, V.Y. Electrophilic-Nucleophilic Dualism of Nickel(II) toward Ni$\cdots$I Noncovalent Interactions: Semicoordination of Iodine Centers via Electron Belt and Halogen Bonding via σ-Hole. *Inorg. Chem.* **2017**, *56*, 13562–13578. [CrossRef]
76. Van Der Bondi, A. Waals Volumes and Radii. *J. Phys. Chem.* **1964**, *68*, 441–451. [CrossRef]
77. Becke, A.D. A New Mixing of Hartree-Fock and Local Density-Functional Theories. *J. Chem. Phys.* **1993**, *98*, 1372–1377. [CrossRef]
78. Barbieri, P.L.; Fantin, P.A.; Jorge, F.E. Gaussian Basis Sets of Triple and Quadruple Zeta Valence Quality for Correlated Wave Functions. *Mol. Phys.* **2006**, *104*, 2945–2954. [CrossRef]
79. MacHado, S.F.; Camiletti, G.G.; Neto, A.C.; Jorge, F.E.; Jorge, R.S. Gaussian Basis Set of Triple Zeta Valence Quality for the Atoms from K to Kr: Application in DFT and CCSD(T) Calculations of Molecular Properties. *Mol. Phys.* **2009**, *107*, 1713–1727. [CrossRef]
80. Campos, C.T.; Jorge, F.E. Triple Zeta Quality Basis Sets for Atoms Rb through Xe: Application in CCSD(T) Atomic and Molecular Property Calculations. *Mol. Phys.* **2013**, *111*, 167–173. [CrossRef]
81. Pritchard, B.P.; Altarawy, D.; Didier, B.; Gibson, T.D.; Windus, T.L. New Basis Set Exchange: An Open, Up-to-Date Resource for the Molecular Sciences Community. *J. Chem. Inf. Model.* **2019**, *59*, 4814–4820. [CrossRef]
82. Frisch, M.J.; Trucks, G.W.; Schlegel, H.B.; Scuseria, G.E.; Robb, M.A.; Cheeseman, J.R.; Scalmani, G.; Barone, V.; Petersson, G.A.; Nakatsuji, H.; et al. *Gaussian 16*; Revision A.03; Gaussian, Inc.: Wallingford, CT, USA, 2016.
83. Wolinski, K.; Hinton, J.F.; Pulay, P. Efficient Implementation of the Gauge-Independent Atomic Orbital Method for NMR Chemical Shift Calculations. *J. Am. Chem. Soc.* **1990**, *112*, 8251–8260. [CrossRef]
84. Lu, T.; Chen, F. Multiwfn: A Multifunctional Wavefunction Analyzer. *J. Comput. Chem.* **2012**, *33*, 580–592. [CrossRef]

85. Chemcraft—Graphical Software for Visualization of Quantum Chemistry Computations. Version 1.8. Available online: www.chemcraftprog.com (accessed on 24 July 2022).
86. *Origin, Version 2018*; OriginLab Corporation: Northampton, MA, USA, 2018.